Lasers in Manufacturing Conference 2023

# Investigations on processing copper-titanium powder blends via PBF-LB/M

Christoph Hecht[a,*], Daniel Schüller[a], Daniel Utsch[a], Thomas Stoll[b], Jörg Franke[a]

[a]*Institute for Factory Automation and Production Systems, Friedrich-Alexander-Universität Erlangen-Nürnberg, Fürther Straße 246b, 90429 Nuremberg, Germany*

[b]*Professorship of Laser-based Additive Manufacturing, TUM School of Engineering and Design, Boltzmannstrasse 15, 85748 Munich, Germany*

**Abstract**

Copper-titanium containing alloys are widely used in active metal brazing of metal-ceramic-joints due to the ability of titanium to wet ceramic components. An important application for such active metal brazed substrates is the production of power electronic circuit carriers, because ceramics, compared to other commonly used insulation materials like epoxy, provide superior characteristics with regard to thermal management and reliability. In this work, a parametric study on processing copper-titanium powder blends with a titanium share of 5 wt.-% and 10 wt.-% via laser-based powder bed fusion of metals is presented. The way of alloying the materials in-situ with the laser is a cost-effective approach to avoid expensive pre-alloyed powders. The study shows suiting process windows to generate samples with a residual porosity of 1 % and less. Additionally, the alloying behavior of the samples is assessed via energy-dispersive X-ray spectroscopy before and after subsequent thermal treatments of the samples.

Keywords: PBF-LB/M; In-Situ Alloying; Copper; Titanium; Active Metal Brazing

## 1. Introduction

Powder bed fusion of metals using a laser-based system (PBF-LB/M) utilizes a focused laser beam to melt layer-wise defined areas of a powder bed according to a geometrical model. The ability to manufacture complex components, which are difficult or impossible to manufacture with conventional subtractive or casting technologies resulted in a strong interest among industrial and scientific communities to utilize PBF-LB/M for new applications and materials. Although the variety of pre-alloyed powders for PBF-LB/M is continuously increasing, customized powder alloys are expensive and lack availability. A promising approach to open up new materials via PBF-LB/M is in-situ alloying of elemental powder blends. By mixing the powders in defined shares, the alloy composition can be customized to the requirements of the application. This

freedom of design and material shows great potential to replace complex process chains and to improve the performance of components. Such a use case is the metallization process of ceramic substrates via direct copper bonding (DBC) and active metal brazing (AMB) for manufacturing high performance power electronic circuit carriers, Stoll et al., 2019. The AMB process utilizes an active filler material, which contains an alloy with commonly up to 10 wt.% of an active element like titanium, zirconium or hafnium to enable wetting of chemically stable ceramic substrates in a brazing process performed under vacuum or inert atmosphere, Pönicke et al., 2011. Common active filler materials are silver-copper-titanium alloys, which are applied as a paste or foil between a ceramic substrate and a copper foil. The alloys are required to provide a lower melting temperature than the joining partners in order to enable brazing without melting the applied copper foils. This restriction can be overcome by utilizing layer-wise additive manufacturing with PBF-LB/M, as the functional copper metallization can be built up on fused and solidified interface material, which has been processed in prior layers.

In order to improve the efficiency of power electronic modules, low ohmic resistances in the electrical load path and low thermal resistances in the thermal path are required. These material properties are determined by the microstructure of the processed parts, Kurdewan, 2022. Since in PBF-LB/M, the material is fused iteratively with a laser, proper process parameters have to be established in order to obtain a dense microstructure with a low amount of porosity. The negative impact of porosity on the electrical properties of additively manufactured copper parts is presented in Stoll et al,. 2020. For proper fusion a suiting amount of energy has to be supplied by the laser. A commonly used quantity to describe the energy input in PBF-LB/M is the volumetric energy density *VED*, which is defined as the ratio of the laser power and the product of the scanning speed *v*, the hatching distance *h* and the layer thickness, Sun et al., 2017. As reported in Giovagnoli et al., 2021, the *VED* is an indicator for a process window, but a detailed consideration of the parameters is required in order to obtain low residual porosity. Besides the residual porosity in the processed material, the metallographic microstructure is of interest for the material properties. For every alloying process, the phase diagram of the investigated material system is of great importance as the material properties are linked to the microstructure of the resulting alloys. For the binary copper-titanium system the phase diagram shows several different phase fields, with different phases occurring ,Soffa and Laughlin, 2004. For a titanium share of up to 10 wt.% besides a phase with dissolved titanium in the copper matrix, an intermetallic $Cu_4Ti$ phase is present. At higher titanium contents further intermetallic phases like $TiCu_2$, $Ti_3Cu_4$ or $Ti_2Cu$ are present in the phase diagram. As with in-situ alloying a powder feed stock of blended elemental powders is iteratively and locally fused with a laser beam at high thermal rates in the range of $10^6$ K/s, Hooper, 2018, a homogeneous alloying as it is obtained in melting furnaces is not guaranteed. This can lead to non-equilibrium phases, which are located in areas of higher titanium content in the phase diagram like $TiCu_2$ or $Ti_3Cu_4$, Dadbakhsh and Hao, 2012. As different phases have different characteristics it is necessary to tailor the microstructure for the desired application. Therefore, fundamental investigations on the porosity formation and alloying behavior of mixed elemental copper and titanium powders in PBF-LB/M are presented in this work.

## 2. Experimental Method

The investigations are split up in two parts. In the first step, process windows for copper-titanium powder blends with 5 wt.% and 10 wt.% titanium are established. The target here is to minimize the residual porosity. In the second step selected samples with low residual porosity are subjected to different heat treatments in order to assess the impact on the alloying behavior.

Both powder blends are mixed from elemental copper ETP powder of manufacturer Ecka Granules and elemental titanium cP Ti powder of manufacturer TLS Technik GmbH & Co. Spezialpulver KG. The copper powder is labeled with AK < 0.045 mm and has a particle size distribution of $d_{10}$ = 11.60 µm and $d_{90}$ = 42.85 µm

according to Stoll 2023. The titanium powder is characterized with a $d_{10}$ of 10 µm and a $d_{90}$ of 45 µm. Both powders have a spherical shape. The blending was performed manually until an optical homogeneous distribution of copper and titanium powder was achieved. The investigations were performed on a Mlab Cusing R of the manufacturer Concept Laser, which is equipped with a fiber laser emitting at a wavelength of 1070 nm up to 500 W. The diameter of the laser spot on the building plate was set to 35 µm. The residual oxygen in the argon flooded process chamber was held below 100 ppm, which was monitored with an Orbitalum ORBMax. During the process, the building plate was actively cooled, which stabilizes the process according to Stoll, 2023. From Stoll, 2023, the detailed machine concept can be obtained as well. The sample geometry is shown in Fig. 1 and is composed of four cylindrical support pillars and a cuboid structure, which is evaluated in the following. Support structures are commonly used for process investigations, Urban et al., 2017, Emminghausen et al., 2019. The samples were exposed with an island strategy. Therefore, the exposure area was divided into squares of 1 mm x 1 mm, which were successively exposed in a random sequence without overlap between the islands. The used build plates are made of copper with a thickness of 10 mm. The samples were separated from the build plates by shearing with a chisel.

Subsequent heat treatments were performed in a Gero Carbolite GHA 12/300 pipe furnace. To create an inert atmosphere of less than 20 ppm of residual oxygen Argon of purity 5.0 was used. Two different heat treatments were conducted. First a solution annealing at 850 °C for 10 hours is performed. A second tempering process was performed at 550 °C for 6 hours. The treatments are derived from Kurdewan and Zilly, 2019. The furnace was heated up with a rate of 10 K/s and passively cooled by switching of the heating element. As shown in Fig. 1, the furnace requires a long time for cooling, because no active cooling is available. The samples were taken out of the furnace at a temperature below 100 °C.

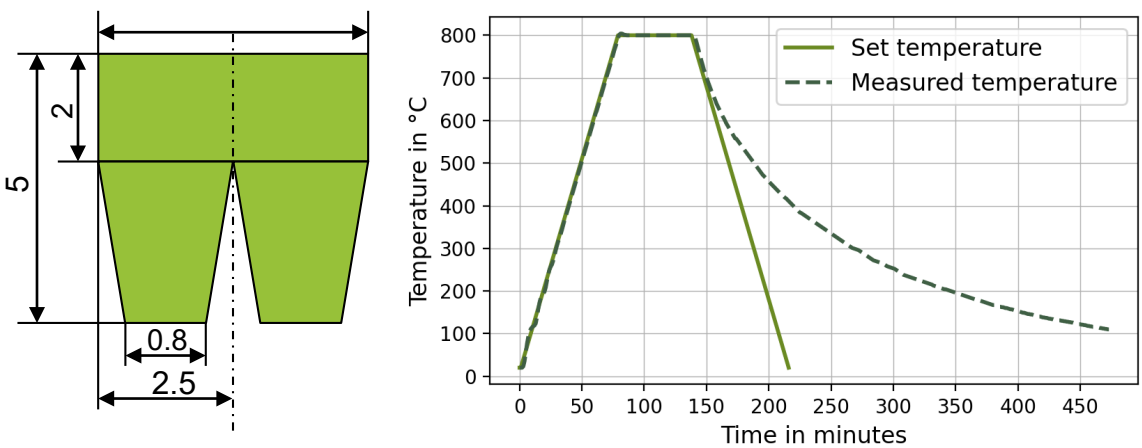


Fig. 1. Sample geometry with in total four pillars as support (left), temperature-time-curve of pipe furnace (right).

To assess the residual porosity and the microstructure, cross-sections of the samples were prepared. Therefore, the samples were embedded in Technovit 4071. Grinding was performed in multiple steps and followed up with polishing in a diamond suspension of 9 µm and 3 µm. For optical microscopy a Leica DVM6 and for energy-dispersive X-ray spectroscopy a Tescan Amber X with a Bruker Quantax200 EDX detector was used. The porosity was assessed in ImageJ after converting the optical microscope image to a greyscale and analyzing the share of black and white pixels. For the measurement, the rectangular top part of the sample was assessed. This way a value for assessing the porosity is obtained VDI, 2013. For each sample one cross-section is analyzed.

## 3. Results and discussion

### *3.1. Establishing a process window with low residual porosity*

The approach on establishing a process window for both powder blends is linked to former investigations on processing pure copper with the same machine set up, Stoll et al., 2020. Here highest densities of over 99.8 % were achieved at *VED* between 750 J/mm$^3$ and 1500 J/mm$^3$. In comparison to copper, titanium has a lower thermal conductivity and the optical absorption at a wavelength of 1070 nm is higher, Mosallanejad et al., 2021. Therefore, lower *VED* compared to pure copper are applied. The process window is established in two steps. In the first step, samples were manufactured at varying parameters as shown in Fig. 2. The samples were then classified according to their optical appearance into deformed samples and samples that lack fusion. All other samples are classified acceptable, and based on the corresponding parameters, the full-factorial experimental designs shown in Table *1* are determined for 5 wt.% and 10 wt.%. In the second step, the experimental designs are carried out. For every parameter combination two samples are manufactured and analyzed. The parameters of the support structures are maintained constant for the two powder blends in order to avoid an influence on the density in the evaluated cuboid area. For 10 wt.% titanium, the parameters of the supports are $P$ = 95 W, $v$ = 600 mm/s, $h$ = 85 µm and for 5 wt.% titanium the parameters of the supports are $P$ = 240 W, $v$ = 700 mm/s, $h$ = 80 µm, leading to a *VED* of 62 J/mm$^3$ and 129 J/mm$^3$. The layer thickness of 30 µm was held constant over all investigations presented in this paper.

The result of the first step to narrow the parameter space is shown in *Fig. 2* for samples with a share of 10 wt.% titanium. Within the yellow bounded area, the samples exhibit a mat appearance. Such behavior of laser melted samples is subjected to a lack of fusion of the particles. The residual porosity of the samples with this fusion characteristic is high. Sun et al., 2017.

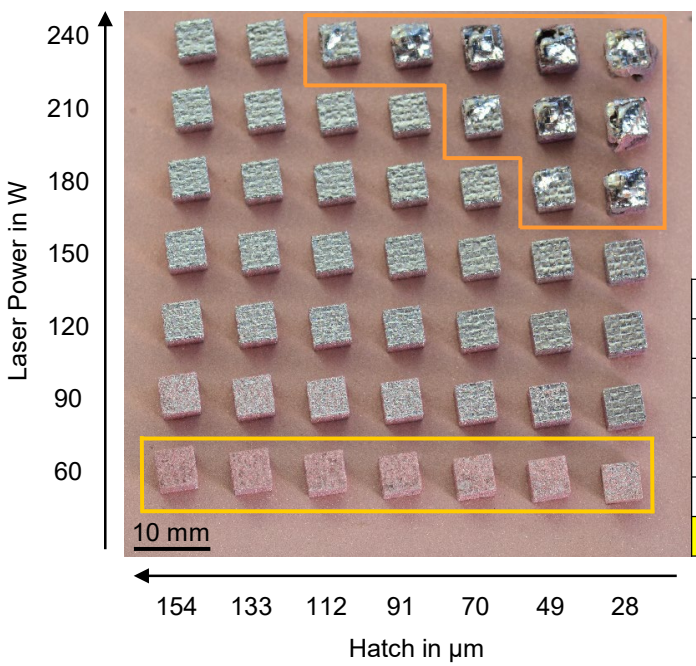


**Classification**

Lack of fusion

Deformation

Corresponding VED in J/mm$^3$, $v$ = 600 mm/s

| | | | | | | |
|---|---|---|---|---|---|---|
| 87 | 100 | 119 | 147 | 190 | 272 | 476 |
| 76 | 88 | 104 | 128 | 167 | 238 | 416 |
| 65 | 75 | 89 | 110 | 128 | 204 | 357 |
| 54 | 63 | 74 | 92 | 119 | 170 | 298 |
| 43 | 50 | 60 | 73 | 95 | 136 | 238 |
| 32 | 38 | 45 | 54 | 71 | 102 | 179 |
| 21 | 25 | 30 | 37 | 48 | 68 | 119 |

Fig. 2. Manual classification based on optical appearance for samples with 10 wt.% titanium.

Table 1. Experimental design.

| Titanium content *s* in wt.% | Laser power *P* in W | Scanning speed *v* in mm/s | Hatch *h* in µm | Range of *VED* in J/mm$^3$ |
|---|---|---|---|---|
| 5 | 100, 130, 160, 190, 220, 250 | 600, 650, 700 | 80, 90, 100 | 48 – 174 |
| 10 | 75, 95, 115 | 600, 650, 700 | 75, 85, 95 | 38 – 85 |

The orange bounded samples are classified as deformed. This behavior is caused by a high energy input and high laser intensity leading to overheating and large melt pools, which results in large geometrical deviations from the target geometry, Kruth et al., 2008. Based on the classification, the wide parameter space is explored iteratively based on the obtained densities of manufactured samples. The initial parameters for 10 wt.% lead to high densities D of over 99.5 % as shown in Fig. 3. For 5 wt.% the parameter space was extended in a first step with 130 W and 160 W of laser power and in a second step with 100 W of laser power.

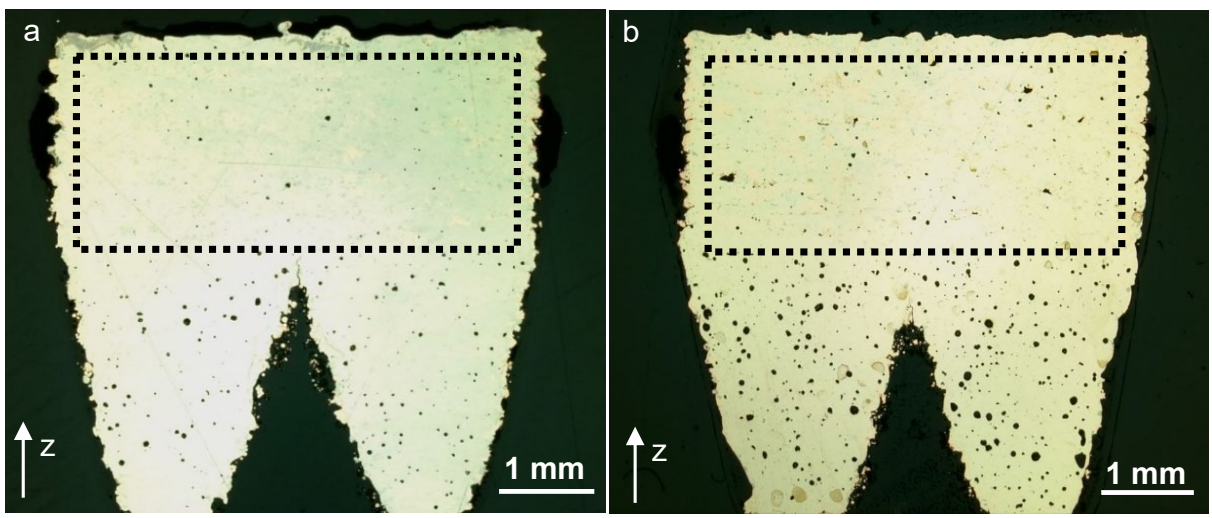


Fig. 3. Regions for optical density analysis; *P* = 115 W, *h* = 95 µm, *v* = 700 mm/s, *s* = 10 wt.%, *D* = 99.64 %, (a); P = 130 W, *h* = 80 µm, *v* = 700 mm/s, *s* = 5 wt.%, *D* = 99.00 % (b).

From Fig. 3 it is possible to observe a difference in the porosity of the cuboid structure and the support structure. This behavior can be related to the thermal boundary conditions, which have a strong influence on the melt pool stability and the different laser parameters used in the two regions. At the notch, where the support structures merge, cracks can be observed in samples of both powder mixtures due to a concentration of thermo-mechanical stresses, Marcelis and Kruth, 2007. For functional parts this has to be considered and prevented by an adapted exposure strategy and part design. The density evaluation of the manufactured samples according to the experimental design in Table 1 is shown in *Fig. 4*. Process windows for both powder blends are defined based on the polynomial trendline of fourth order. For 5 wt.% samples of more than 98 % density can be obtained by volumetric energy densities between 70 J/mm$^3$ and 90 J/mm$^3$. Within the investigation one sample with a density of 99.00 % was achieved, which is shown in Fig. 3b. For 10 wt.% titanium samples of more than 99 % density are obtained by volumetric energy densities between 51 J/mm$^3$ and 77 J/mm$^3$. The sample with the highest density reached 99.78 % and was obtained by *P* = 95 W, *v* = 650 mm/s and *h* = 85 µm. In comparison, the powder with a titanium share of 10 wt.% can be processed

to samples with higher densities in the considered experimental design. This can be subjected to melt pool instabilities, which are related to the higher content of copper, which leads to a higher thermal conductivity of the processed samples.

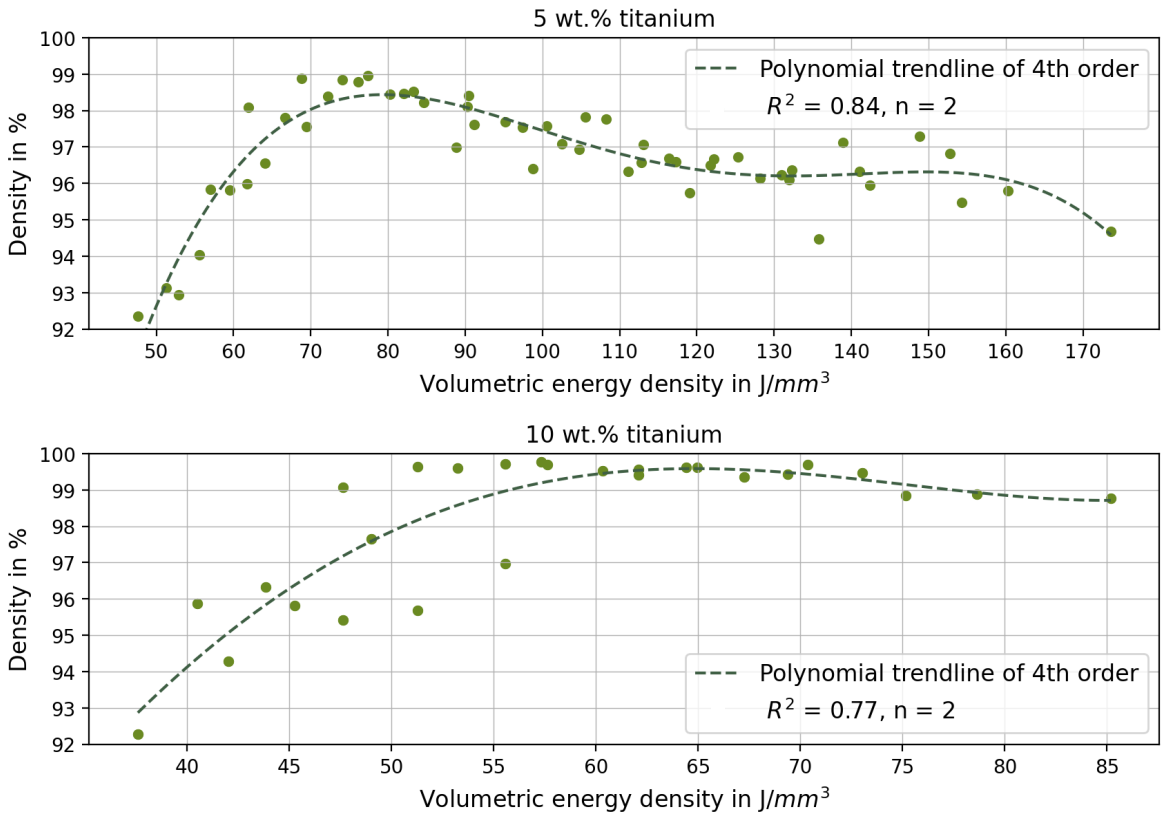


Fig. 4. Obtained densities in dependence of the volumetric energy density.

The process window is bounded by the formation of residual porosity of different character. At high VED, keyholes build up and collapse repeatedly, which leads to spherical porosities. The high porosity in the support structures of samples with 5 wt.% titanium can be subjected to the same relationship as the applied volumetric energy density of 130 J/mm$^3$ in support region exceeds the process window significantly. At lower VED the particles are not molten up properly and the layers lack fusion. This can also be observed in Fig. 5d for a titanium share of 10 wt.%. Despite the formation of porosities, the alloying behavior of the elemental powder blends can be observed in Fig. 5 as well. With decreasing VED, the samples show increasing areas of copper and grey-colored titanium. This implies that at higher VED alloying is improved. At high densities of over 99 % no homogeneous colored samples are obtained, as similar to Fig. 5b grey titanium particles are still observable for all samples.

The *VED* as a characteristic value to predict the density is limited. In Fig. 4 for example a *VED* of 55.6 J/mm$^3$ leads to a density of over 99 % as well as to a density of less than 97 %. Therefore, it is necessary to evaluate the impact of all parameters separately. The main effects of the parameters are shown in Fig. 6 for both

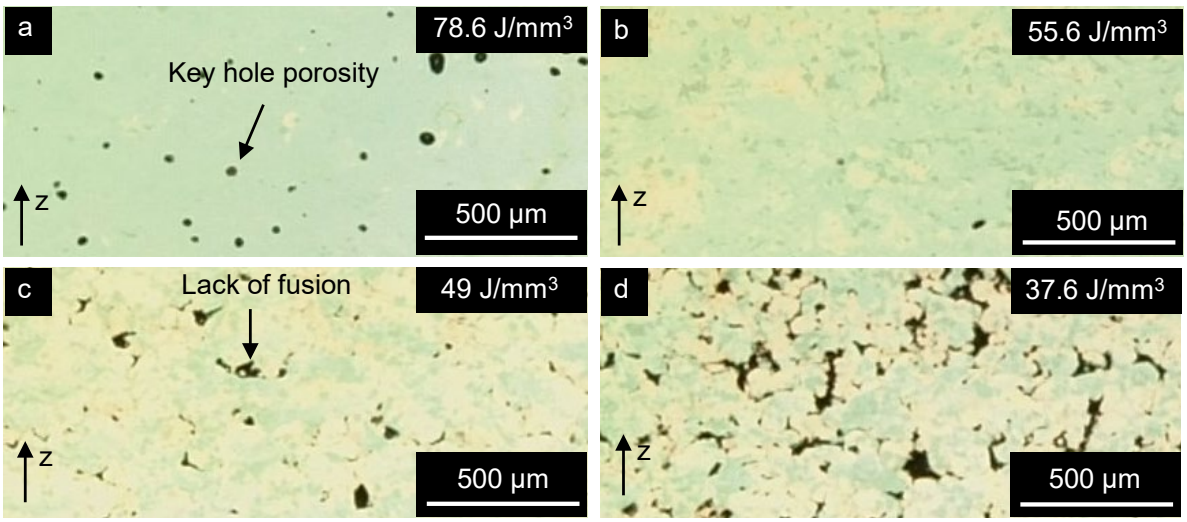


Fig. 5. Cross-sections of samples with 78.6 J/mm³ (a), 55.6 J/mm³ (b), 49 J/mm³ (c), 37.6 J/mm³ (d) and s = 10 wt.%.

powder blends. Within the investigated parameter range, the laser power has the strongest impact on the density. Statistically significant for 10 wt.% titanium is the scan speed and for 5 wt.% the hatch. Furthermore, both two factor interactions containing the laser power are significant as well.

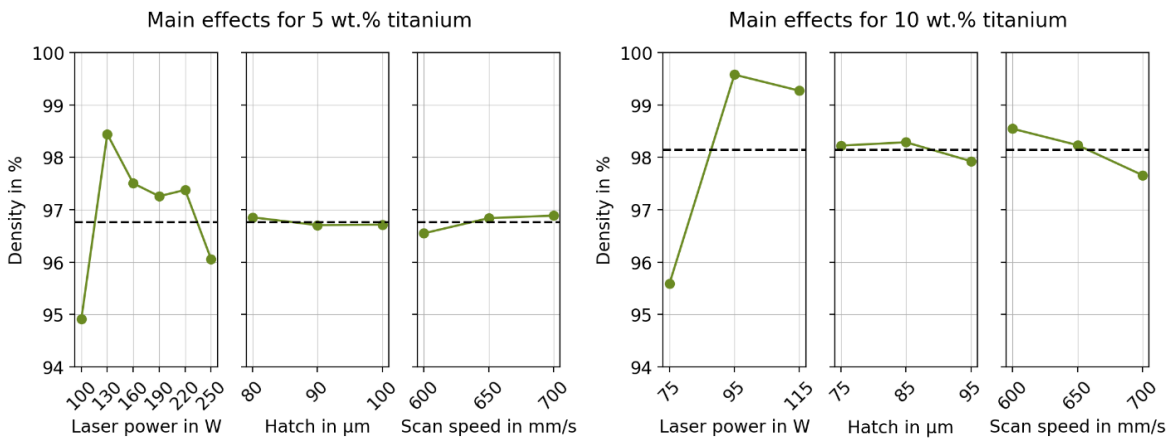


Fig. 6. Evaluation of the main effects on the density according to the experimental design in Table 1.

### *3.2. Heat treatment*

Based on the obtained knowledge from Fig. 6, that a higher degree of alloying via PBF-LB/M is related to the formation of porosities, subsequent heat treatments are performed on a sample within in the defined process window for 5 wt.% titanium according to Table 2 and section 2.

Table 2. Experimental design for heat treatments of samples manufactured at $P$ = 130 W, $h$ = 90 µm, $v$ = 600 mm/s, $s$ = 5 wt.% titanium, $VED$ = 72 J/mm$^3$, $D$ = 98.38%.

| Term | a | b | c | d |
|---|---|---|---|---|
| Heat treatment | - | 850 °C/10 h | 550 °C/6 h | 850 °C/10 h + 550 °C/6 h |

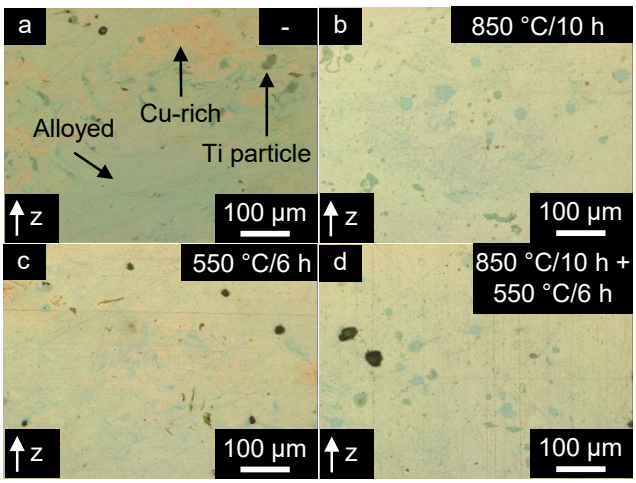


Fig. 7. Microscopic images of cross-sections after thermal treatment according to Table 2.

In Fig. 7 the effect of the heat treatment on the material structure is shown. Analogous to the samples in Fig. 5b with 10 wt.% titanium, the microstructure of samples without heat treatment is very inhomogeneous. The microstructure can be classified into the three categories copper-rich, titanium-rich and alloyed areas. The titanium-rich areas are composed of undissolved particles, which can be related to an insufficient melting and alloying. An important aspect for this behavior is the thermo-physical properties of titanium and copper. Titanium has a melting point of 1668 °C and copper melts at 1085 °C. At 1668 °C copper has a viscosity of 1.96 mPas, which is lower compared to 4.42 mPas of titanium at the same temperature. Within the short melting interval improper alloying of the viscous titanium particles in the low viscosity copper phase occurs. Yadroitsev et al., 2017.

The heat-treated samples still show an inhomogeneous microstructure with undissolved titanium particles. At 550 °C coarse titanium particles are not observed and copper-rich areas are smaller. This leads to the assumption, that titanium spreads out in a solid-state diffusion process. At 850 °C, despite the absence of copper-rich areas, larger titanium particles are observable. When the thermal treatment at 850 °C is followed up with a thermal treatment at 550 °C according to Table 2, the enlarged titanium particles are still obtained. So, the effect of the thermal treatment at 550 °C seems to depend on prior heat treatments.

The alloying behavior of the heat-treated samples was further assessed with EDX-analysis. Table 3 shows the detected copper and titanium shares of the samples shown in Fig. 8. The titanium share deviates between 0.85 and 1.25 weight percentage points from the target value of 5 wt.%. This can be subjected to particle segregation during pre-processing steps as the density of copper is almost twice as high as the density of titanium, Yadroitsev et al., 2017, or insufficient mixing of the elemental blends. Based on Fig. 8a, a distinction between copper-rich and alloyed areas as it is possible based on the optical micrograph in Fig. 7a is not possible. Fig. 8 confirms the observation that a treatment of 550 °C improves the alloying, as less undissolved particles are observed. Nevertheless, undissolved particles are still present.

Table 3 Obtained total shares of copper and titanium in EDX-analysis in Table 2.

| Heat treatment | a | b | c | d |
|---|---|---|---|---|
| Titanium share | 5.85 wt.% | 5.99 wt.% | 6.25 wt.% | 5.99 wt.% |
| Copper share | 94.15 wt.% | 94.01 wt.% | 93.75 wt.% | 94.01 wt.% |

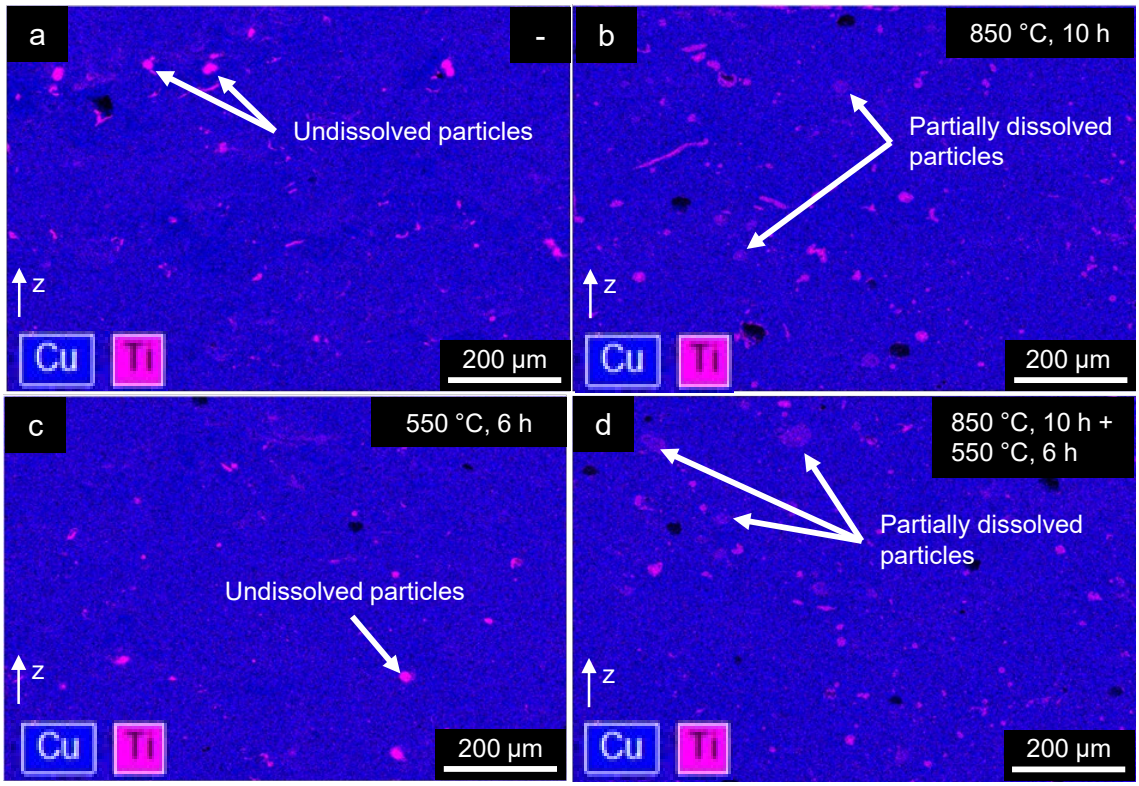


Fig. 8. EDX analysis of titanium and copper distribution in heat-treated samples according to Table 2.

An enlargement of the undissolved particles after a treatment at 850 °C can partially be observed as the contrast of some titanium particles is decreasing. By applying a thermal treatment at 850 °C followed up with a treatment at 550 °C, this behavior intensifies as some titanium particles in Fig. 8d have a low contrast in the EDX map and spread over a larger area.

**4. Summary**

In this study elemental powder blends of copper with 5 wt.% and 10 wt.% titanium have been processed by means of laser powder bed fusion at a wavelength of 1070 nm. The conducted full factorial design focused on the volumetric energy density to manufacture samples of high density by taking the laser power, the hatching distance and the scanning speed into account. By fitting a polynomial trendline to the measured densities, process windows for both powder blends are defined. For a share of 10 wt.% titanium, samples of densities higher than 99 % were achieved at volumetric energy densities between 51 J/mm$^3$ and 77 J/mm$^3$. At a share of 5 wt.% titanium densities higher than 98 % were obtained at volumetric energy densities between 70 /mm$^3$ and 90 J/mm$^3$. Higher volumetric energy densities favor the formation of a homogeneous alloy but also lead to spherical key hole porosities. Volumetric energy densities within the identified process windows of the two powder blends lead to an inhomogeneous alloying behavior with undissolved titanium particles. Thermal treatment at 550 °C and 850 °C showed potential to dissolve titanium but with the applied dwell times titanium particles were not dissolved completely. By applying a heat treatment at 850 °C and following up with

a treatment at 550 °C a dissolution process of titanium particles was observed in EDX analysis. To avoid undissolved titanium particles further investigations with a heated building plate, Martinez et al., 2019, a larger laser spot, Yadroitsev et al., 2017, and double laser exposure, Huber et al., 2021, are promising approaches.

## Acknowledgements

Funded by the Deutsche Forschungsgemeinschaft (DFG, German Research Foundation) – 434962551; 442921285.

## References

Dadbakhsh S, Hao L, 2012. Effect of Al alloys on selective laser melting behaviour and microstructure of in situ formed particle reinforced composites. Journal of Alloys and Compounds, 541, 328–334.

Emminghausen, J., Hoff, C., Hermsdorf, J., Kaierle, S., 2019. Additive manufacturing of CuSn10 Powder via selective laser melting. In Proceedings of Lasers in Manufacturing (LiM), Munich, Germany.

Giovagnoli, M., Silvi, G., Merlin, M., Di Giovanni, M., T., 2021. Optimisation of process parameters for an additively manufactured AlSi10Mg alloy: Limitations of the energy density-based approach on porosity and mechanical properties estimation. Materials Science and Engineering: A, 802, 140613

Hooper, P., A., 2018. Melt pool temperature and cooling rates in laser powder bed fusion. Additive Manufacturing, 22, pp. 548–559. https://www.sciencedirect.com/science/article/pii/S221486041830188X

Huber, F., Rasch, M., Schmidt, M., 2021. Laser Powder Bed Fusion (PBF-LB/M) Process Strategies for In-Situ Alloy Formation with High-Melting Elements. Metals, 11 (2), p. 336.

Kurdewan, T., Zilly, A., 2019. Kupferlegierungen mit Titan–Wirkmechanismen geringer Legierungsanteile in Werkstoffen mit hoher Festigkeit und guter Leitfähigkeit. Metall, 73(11), pp. 436-439.

Kruth, J-P., Mercelis, P., van Vaerenbergh, J., Craeghs, 2007. Feedback control of selective laser melting. In Proceedings of the 3rd International Conference on Advanced Research in Virtual and Rapid Prototyping, Portugal, pp. 521–527.

Kurdewan, T., 2022. Beitrag zur Eigenschaftsoptimierung von ausscheidungshärtbaren niedriglegierten Kupfer-Titan-Legierungen.

Marcelis, P., Kruth, J-P., 2007. Residual stresses in selective laser sintering and selective laser melting. Rapid Prototyping Journal, 12 (5), 254–265.

Martinez, R., Todd, I., Mumtaz, K., 2019. In situ alloying of elemental Al-Cu12 feedstock using selective laser melting. Virtual and Physical Prototyping, 14 (3), pp. 242–252.

Mosallanejad, MH., Niroumand, B., Aversa, A., Manfredi, D., Saboori, A., 2021. Laser Powder Bed Fusion in-situ alloying of Ti-5%Cu alloy: Process-structure relationships. Journal of Alloys and Compounds, p. 857.

Pönicke, A., Schilm, J., Böhm, G., Schnee, D., 2011. Aktivlöten von Kupfer mit Aluminiumnitrid-und Siliziumnitridkeramik. Keramische Zeitschrift, 65 (5), 334–342.

Soffa, W., A., Laughlin, D., E., 2004. High-strength age hardening copper–titanium alloys: redivivus. Progress in Materials Science, 49 (3-4), pp. 347–366.

Stoll, T., 2023. Laser Powder Bed Fusion von Kupfer auf Aluminiumoxid-Keramiken. FAU Studien aus dem Maschinenbau Band 420. Erlangen: FAU University Press. DOI: 10.25593/978-3-96147-632-9.

Stoll, T., Kirstein, M., Franke, J., 2019. A novel approach of copper-ceramic-joints manufactured by selective laser melting. In: Material Technologies and Applications to Optics, Structures, Components, and Sub-Systems IV. Vol. 111101.SPIE, p. 53–63.

Stoll, T., Trautnitz, P., Schmiedeke, S., Franke, J., Travitzky, N., 2020. Process development for laser powder bed fusion of pure copper. In: Gu, B., Chen, H., Helvajian, H. (eds.). Laser 3D Manufacturing VII. 4-6 February, 2020, San Francisco, California, United States, 2/1/2020 - 2/6/2020. SPIE, Bellingham, Washington, USA, p. 46.

Sun, S., Brandt, M., Easton, M., 2017. Powder bed fusion processes: an overview. In: Brandt M (ed.). Laser additive manufacturing. Materials, design, technologies, and applications. Elsevier/Woodhead Publishing Woodhead Publishing is an imprint of Elsevier, Amsterdam, p. 55–77.

Urban, N., Huber, F., Franke, J., 2017. Influences of process parameters on rare earth magnets produced by laser beam melting. In Proceedings of the 7th International Electric Drives Production Conference (EDPC). Wuerzburg, Germany, pp. 1–5.

VDI Guideline 3405, Part 2, 2013. Additive manufacturing processes, rapid manufacturing beam melting of metallic parts. Qualification, quality assurance and post processing. Beuth, Berlin.

Yadroitsev, I., Krakhmalev, P., Yadroitsava, I., 2017. Titanium Alloys Manufactured by In Situ Alloying During Laser Powder Bed Fusion. JOM, 69 (12), pp. 2725–2730.